Structural dynamics of protein backbone ψ angles: Extended molecular dynamics simulations versus experimental 3J scalar couplings

5 AUTHORS, INCLUDING:

Guillaume Bouvignies
Ecole Normale Supérieure de Paris
35 PUBLICATIONS **991** CITATIONS

COMMUNICATION

Structural dynamics of protein backbone φ angles: extended molecular dynamics simulations versus experimental ^3J scalar couplings

Phineus R. L. Markwick · Scott A. Showalter · Guillaume Bouvignies · Rafael Brüschweiler · Martin Blackledge

Abstract ^3J scalar couplings report on the conformational averaging of backbone φ angles in peptides and proteins, and therefore represent a potentially powerful tool for studying the details of both structure and dynamics in solution. We have compared an extensive experimental dataset with J-couplings predicted from unrestrained molecular dynamics simulation using enhanced sampling available from accelerated molecular dynamics or using long timescale trajectories (200 ns). The dynamic fluctuations predicted to be present along the backbone, in agreement with residual dipolar coupling analysis, are compatible with the experimental ^3J scalar couplings providing a slightly better reproduction of these experimental parameters than a high resolution static structure.

Proteins are intrinsically flexible, exhibiting dynamics over a range of time scales from pico-seconds to seconds. This flexibility allows conformational changes in protein backbone and sidechains to play crucial roles in biomolecular function. NMR spectroscopy provides a wealth of information on protein dynamics occurring over a vast range of timescales (Mittermaier and Kay 2006). Residual dipolar couplings (RDCs) (Tjandra and Bax 1997; Tolman et al.

1995) and ^3J scalar couplings (Case 2000; Schmidt et al. 1999) both report on time- and ensemble averages whose interconversion rates may extend into the millisecond range, rendering these parameters sensitive to the same types of protein motions.

Diverse approaches have been proposed to determine dynamic amplitudes and anisotropies of individual bond vectors or local structural motifs from multiple RDC measurements (Yao et al. 2008a, b; Meiler et al. 2001; Clore and Schwieters 2004; Ulmer et al. 2003; Bernado and Blackledge 2004a, b; Bouvignies et al. 2005, 2006; Tolman 2002; Showalter and Brüschweiler 2007a, b; Lakomek et al. 2008, Salmon et al. 2009, Yao et al. 2008a, b; Vogeli et al. 2008). Vicinal scalar couplings report on the conformational sampling of torsion angles φ following empirical relationships of the form (Karplus 1959).

$$\langle ^3J\rangle = A\langle\cos^2(\varphi + \theta)\rangle + B\langle\cos(\varphi + \theta)\rangle + C \qquad (1)$$

where the angular brackets indicate time and ensemble averaging. The conformational dependence of (1) makes these parameters highly complementary to residual dipolar couplings, providing the perspective, for example, of correlating the motions of adjacent peptide planes, via φ- and ψ-dependent ^3J-couplings and orientation-dependent RDCs.

The main obstacle for the direct conversion of measured ^3J-couplings into geometric information is the availability of Karplus parameters A, B, C for different types of ^3J-coupling constants. Despite advances in quantum-chemical calculations for the prediction of these parameters, standard applications often employ empirically parametrized Karplus-type relationships derived from experimental ^3J-couplings of proteins with known average structure. The Karplus parameters are assumed to be independent of the amino-acid types and thus side-chain specific substituent

P. R. L. Markwick · G. Bouvignies · M. Blackledge (✉)
Protein Dynamics and Flexibility, Institut de Biologie
Structurale Jean-Pierre Ebel UMR 5075, CNRS/CEA/UJF,
41 Rue Jules Horowitz, 38027 Grenoble, France
e-mail: martin.blackledge@ibs.fr

S. A. Showalter · R. Brüschweiler (✉)
Department of Chemistry and Biochemistry, NHMFL, Florida
State University, Tallahassee, FL 32306, USA
e-mail: bruschweiler@magnet.fsu.edu

effects are ignored. Moreover, since such empirically derived Karplus parameters absorb motional effects of the protein used for calibration, they are not directly applicable to the quantitative characterization of dihedral angle dynamics in other proteins (Brüschweiler and Case 1994).

On the theoretical side, molecular dynamics (MD) simulations can assist the structural and dynamic interpretation of experimental scalar J-couplings on the ps to sub-µs range (Hoch et al. 1985; Brüschweiler and Case 1994). ^3J-couplings have been used to probe the extent of conformational sampling of the protein backbone by combining experimental measurement with molecular dynamics (MD) simulation and DFT calculation (Case et al. 2000). A recent study used a set of three φ-dependent scalar couplings {$^3J_{HNH\alpha}$, $^3J_{HNC'}$, $^3J_{HNC\beta}$} to propose limits on the extent of backbone motion present in the protein GB3 (Vogeli et al. 2007). In this study, Karplus parameters were optimized from experimental couplings and backbone dihedral angles present in a high resolution structural model (Ulmer et al. 2003). This protein has attracted intense scrutiny regarding the nature and extent of the flexibility along its peptide backbone. The RDCs measured in multiple alignment media that were used to determine the high-resolution structure have been interpreted using the three-dimensional Gaussian axial fluctuation (GAF) motional model (Bouvignies et al. 2005). They provided evidence for a heterogeneous distribution of slow (ns–ms) timescale motions over the protein backbone, with detectable slower motions present in loop I and in the β-strand, but negligible additional motions elsewhere (Bouvignies et al. 2006). This dynamic distribution was also closely reproduced by accelerated molecular dynamics (AMD) simulation (Markwick et al. 2007), an approach that enhances conformational sampling in molecular simulations by artificially lowering transition barriers between energy substates (Hamelberg et al. 2004). The success by which AMD reproduces the RDCs attests to its ability to sample processes approaching the ms time scale.

In this communication we investigate the ability of structural ensembles generated by AMD and standard MD trajectories to reproduce the three types of scalar J-coupling constants {$^3J_{HNH\alpha}$, $^3J_{HNC'}$, $^3J_{HNC\beta}$}, and compare this to the reproduction achieved when using a single structure refined with experimental RDCs. Different levels of conformational sampling were achieved by generating multiple ensembles of protein G: either averaging 2 ns trajectories sampled from different starting points across the AMD and resampling on the basis of the 'free energy' to provide a canonical ensemble, or using multiple 2 ns MD trajectories starting from the X-ray crystal structure. The former approach has broader sampling with respect to the average structure (backbone rmsd 0.73 ± 0.16 Å compared to 0.54 ± 0.09 Å). In order to determine optimal

Karplus parameters [A, B, C and θ in (1)], all conformations in the relevant ensemble were combined and the most appropriate parameters determined by fitting to experimental data.

The fitting approach used here to extract the optimal Karplus parameters from (1) is an adaptation of the singular value decomposition (SVD) approach for the dynamic interpretation of RDCs from MD trajectories (Losonczi and Prestegard 1998; Showalter and Brüschweiler 2007a, b). Since motional averaging only affects the cosine functions, the fitted Karplus parameters do not include any motional effects. For comparison, the SVD fitting was also applied using the single static structure (pdb code 2oed). Analysis of the AMD ensemble and 2oed are compared in Fig. 1 with the results summarized in Table 1. They show that a similarly good reproduction of experimental data is obtained for static and dynamic fitting. Data were removed for 5 out of 48 sites for which generalised order parameters for NH^N and C′C$^\alpha$ vectors determined using 3DGAF analysis of the experimental RDCs were violated ($|\Delta S_{rdc}^2| > 0.15$) by the AMD ensemble (Markwick et al. 2007). The rmsd of the $^3J_{HNH\alpha}$ couplings is 0.61 Hz for the static case, 0.64 Hz for the MD simulations from the relaxed crystal structure and 0.56 Hz for the simulations whose initial structures were extracted from the AMD sampling. It is notable that the largest improvements in the reproduction of the remaining $^3J_{HNH\alpha}$ and $^3J_{HNC'}$ appear in the loop I/β2 region (Leu 17 and Lys 18) and Asp 45, regions (Fig. 2) where the highest
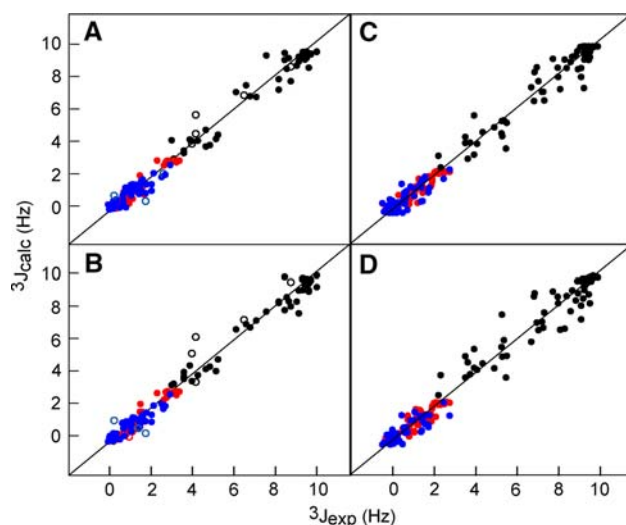

Fig. 1 Reproduction of $^3J_{HNH\alpha}$ (*black*), $^3J_{HNC'}$ (*blue*), $^3J_{HNC\beta}$ (*red*) scalar couplings from GB3 using **A** the static structure (2oed) **B** conformational ensembles derived from 60 2 ns fully solvated MD simulations seeded from the enhanced conformational space sampling AMD simulations. *Open circles* indicate points for which $\left|\Delta S_{rdc}^2\right| > 0.15$ (see text). **C** Reproduction of experimental J-couplings of ubiquitin by calculations from the static structure (1d3z) and from **D** 200 ns unrestrained MD simulation

Table 1 Reproduction of $^3J_{HNH\alpha}$, $^3J_{HNC'}$ and $^3J_{HNH\beta}$ using static and dynamic descriptions of GB3

	Rmsd (Hz)	A (Hz)	B (Hz)	C (Hz)	θ (°)[c]
$^3J_{HNH\alpha}$					
Static[a]	0.63 (0.61)[d]	7.76	−1.25	0.73	−61
MD[a]	0.73 (0.64)	9.95	−1.44	−0.95	−63
AMD[a]	0.64 (0.56)	10.35	−1.59	−1.15	−63
Static[b]	0.72	7.09	−1.42	1.55	−60
MD[b]	1.04	7.74	−1.48	1.18	−60
LMD[b]	0.88	8.30	−1.55	0.74	−60
$^3J_{HNC'}$					
Static[a]	0.40 (0.36)	4.01	−1.33	0.24	178
MD[a]	0.44 (0.36)	4.63	−1.46	−0.21	179
AMD[a]	0.41 (0.35)	5.07	−1.68	−0.25	179
Static[b]	0.43	4.29	−1.01	0.00	180
MD[b]	0.52	4.65	−1.55	−0.20	180
LMD[b]	0.43	5.07	−1.63	−0.28	180
$^3J_{HNC\beta}$					
Static[a]	0.27 (0.27)	4.05	−0.84	0.16	57
MD[a]	0.34 (0.33)	3.81	−0.74	0.19	57
AMD[a]	0.31 (0.30)	3.46	−0.59	0.24	59
Static[b]	0.31	3.06	−0.74	0.13	60
MD[b]	0.61	2.58	−0.34	0.21	60
LMD[b]	0.34	2.84	−0.44	0.12	60
$^3J_{HNH\alpha}$ "zero motion"[e]		9.5	−1.4	0.3	−60
$^3J_{HNH\alpha}$ DFT1[f]		9.44	−1.53	−0.07	−60
$^3J_{HNC'}$ DFT1[f]		5.58	−1.06	−0.30	180
$^3J_{HNC\beta}$ DFT1[f]		5.15	0.01	−0.32	60

MD, AMD and LMD refer to standard (2 ns), accelerated and long (200 ns) timescale molecular dynamics simulations, respectively

[a, b] Analyses refer to GB3 and ubiquitin, respectively

[c] θ was not optimized for ubiquitin

[d] Values in parentheses refer to sites for which $\left|\Delta S^2_{rdc}\right| < 0.15$. All simulations used AMBER8 (Case et al. 2005) with the AMBER99SB force field (Hornak et al. 2006)

[e] Values of Karplus parameters extrapolated to "zero motion" in the study of Brüschweiler and Case (1994)

[f] Values of Karplus parameters determined from DFT calculations (Case et al. 2000)

amplitude dynamics are found from RDC analysis (Fig. 3). A similar level of reproduction of $^3J_{HNC\beta}$ and $^3J_{HNC'}$ couplings is found for all three cases. In general then we find that the significant dynamics found in the interaction site in the loop I/β2 region, both experimentally from RDCs and from AMD simulation, are in good agreement with the measured J-couplings.

The same type of analysis has been performed on the protein ubiquitin, comparing the static structure (1ubq), short (2 ns), and long (200 ns) (Showalter and Brüschweiler 2007a, b) MD simulations to experimental couplings (Hu and Bax 1996) (Fig. 1; Table 1). Although the
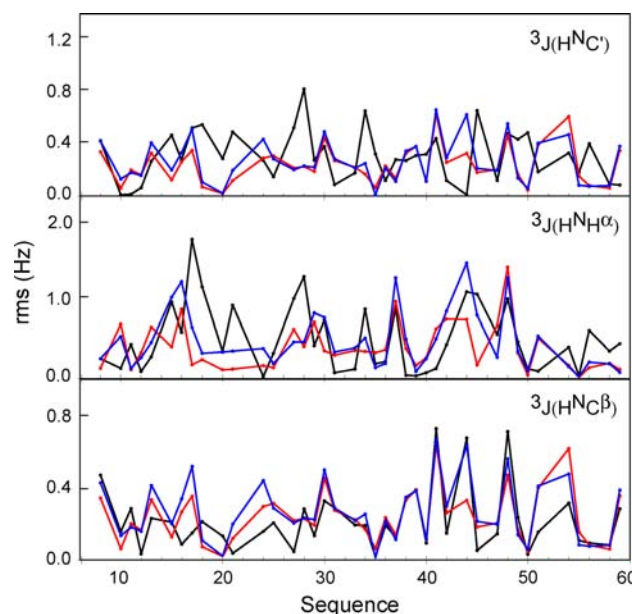

Fig. 2 Reproduction of the $^3J_{HNH\alpha}$, $^3J_{HNC'}$, $^3J_{HNC\beta}$ scalar couplings of GB3 using the static structure 2oed (*black*) compared to the average improvement derived using 60 2 ns fully solvated MD simulations from the relaxaed crystal structure (*blue*) and the 60 2 ns fully solvated MD simulations from different regions of conformational space sampled over the AMD simulation (*red*)

precision of the J-couplings measured for ubiquitin is lower than for GB3, static and dynamic analyses reproduce the data with similar accuracy.

In Fig. 4 we compare Karplus parameters for the two couplings, $^3J_{HNH\alpha}$ and $^3J_{HNC'}$, for which systematic differences in Karplus parameters are found between dynamic and static analyses. The analyses that explicitly account for dynamic averaging tend towards the DFT-derived relationships in the region $\varphi < -50°$ (Case et al. 2000), while principal differences between LMD and AMD-derived curves are found in φ ranges that are underrepresented in both GB3 and ubiquitin ($\varphi > -50°$).

Enhanced conformational sampling from both AMD and long time-scale MD simulations reproduce dynamic modes observed from experimental RDCs and therefore describe the main angular fluctuations that may occur up to the millisecond range. ^3J-scalar couplings report on averages over similar timescales as RDCs, so that the same sampling techniques can be used to investigate dynamic averaging of both parameters. Extraction of quantitative dynamic information from these data is complicated by the absence of independent reference parameters for the Karplus relationships and the fact that local motion may also be absorbed into effective Karplus parameters, further limiting sensitivity to dynamic detail. Nevertheless, despite these theoretical drawbacks, the fact that unrestrained dynamic ensembles reproduce experimental values as well as, and sometimes better than, high-resolution static structures

Fig. 3 Order parameters for the (*top*) AMD simulation of protein G (Markwick et al. 2007), (*bottom*) 200 ns MD simulation of ubiquitin (Showalter and Brüschweiler 2007a, b), which were used for the analysis of ^3J couplings
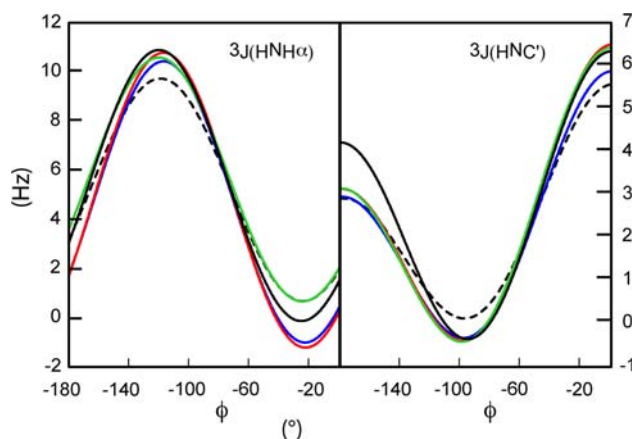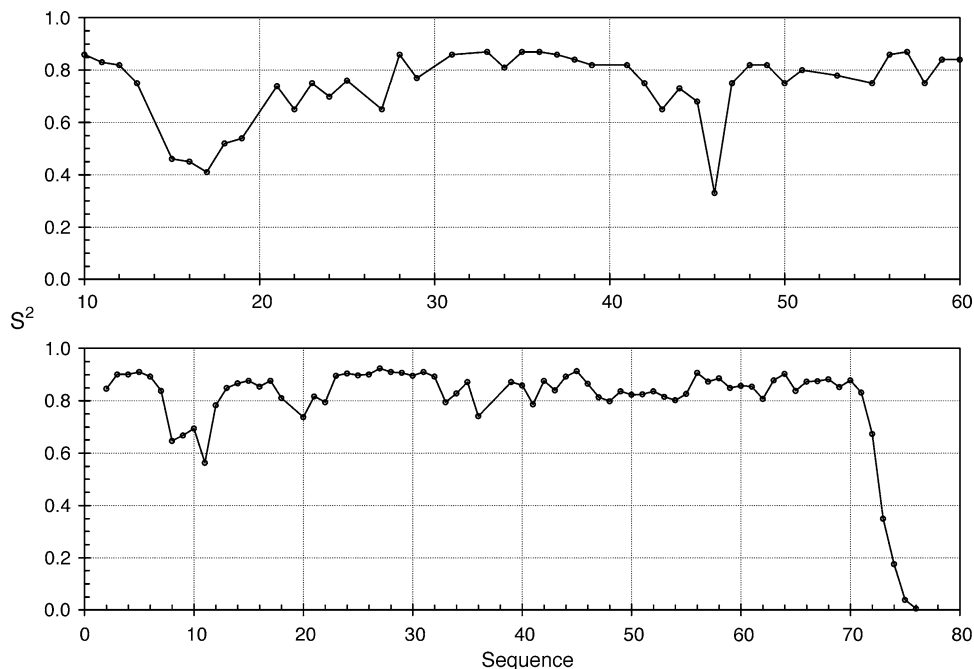

Fig. 4 Comparison of Karplus curves shown in Table 1 over the range $-180° < \varphi < 0°$ for $^3J_{HNH\alpha}$ (*left*) and $^3J_{HNC'}$ (*right*) scalar couplings. *Dashed line*: static structure analysis, *blue* MD analysis, *red* AMD analysis, *green* LMD analysis of ubiquitin. *Solid black line* DFT1 Karplus parameters from Case et al. (2000) (see Table 1)

refined against NMR data is noteworthy. The analysis presented here indicates that the φ-dihedral angle fluctuations along the protein backbones of GB3 and ubiquitin predicted by extended and accelerated MD simulations are on average compatible with the experimental scalar ^3J couplings provided that the Karplus parameters are optimized accordingly. Interestingly, the optimized Karplus parameters turn out to be very similar to the parameters that were previously obtained from density functional theory (DFT).

References

Bernado P, Blackledge M (2004a) Anisotropic small amplitude peptide plane dynamics in proteins from residual dipolar couplings. J Am Chem Soc 126:4907–4920

Bernado P, Blackledge M (2004b) Local dynamic amplitudes on the protein backbone from dipolar couplings: toward the elucidation of slower motions in biomolecules. J Am Chem Soc 126:7760–7761

Bouvignies G, Bernado P, Meier S, Cho K, Grzesiek S, Brüschweiler R, Blackledge M (2005) Identification of slow correlated motions in proteins using residual dipolar and hydrogen-bond scalar couplings. Proc Natl Acad Sci USA 102:13885–13890

Bouvignies G, Markwick P, Brüschweiler R, Blackledge M (2006) Simultaneous determination of protein backbone structure and dynamics from residual dipolar couplings. J Am Chem Soc 128:15100–15101

Brüschweiler R, Case D (1994) Adding harmonic motion to the Karplus equation for spin–spin coupling. J Am Chem Soc 116:11199–11200

Case DA (2000) Interpretation of chemical shifts and coupling constants in macromolecules. Curr Opin Struct Biol 10:197–203

Case DA, Scheurer C, Brüschweiler R (2000) Static and dynamic effects on vicinal scalar J couplings in proteins and peptides: a MD/DFT analysis. J Am Chem Soc 122:10390–10397

Case DA, Cheatham TE 3rd, Darden T, Gohlke H, Luo R, Merz KM Jr, Onufriev A, Simmerling C, Wang B, Woods RJ (2005) The amber biomolecular simulation programs. J Comput Chem 26:1668–1688

Clore GM, Schwieters CD (2004) How much backbone motion in ubiquitin is required to account for dipolar coupling data measured in multiple alignment media as assessed by independent cross-validation? J Am Chem Soc 126:2923–2938

Hamelberg D, Mongan J, McCammon JA (2004) Accelerated molecular dynamics: a promising and efficient simulation method for biomolecules. J Chem Phys 120:11919–11929

Hoch JC, Dobson CM, Karplus M (1985) Vicinal coupling constants and protein dynamics. Biochemistry 24:3831–3841

Hornak V, Okur A, Rizzo RC, Simmerling C (2006) HIV-1 protease flaps spontaneously open and reclose in molecular dynamics simulations. Proc Natl Acad Sci U S A 103:915–920

Hu J-S, Bax A (1996) Measurement of three-bond ^{13}C-^{13}C J couplings between carbonyl and carbonyl/carboxyl carbons in isotopically enriched proteins. J Am Chem Soc 118:8170–8171

Karplus M (1959) Contact electron-spin coupling of nuclear magnetic moments. J Chem Phys 30:11–15

Lakomek NA, Walter KF, Fares C, Lange OF, de Groot BL, Grubmuller H, Brüschweiler R, Munk A, Becker S, Meiler J, Griesinger C (2008) Self-consistent residual dipolar coupling based model-free analysis for the robust determination of nanosecond to microsecond protein dynamics. J Biomol NMR 41:139–155

Losonczi JA, Prestegard JH (1998) Improved dilute bicelle solutions for high-resolution NMR of biological macromolecules. J Biomol NMR 12:447–451

Markwick PR, Bouvignies G, Blackledge M (2007) Exploring multiple timescale motions in protein GB3 using accelerated molecular dynamics and NMR spectroscopy. J Am Chem Soc 129:4724–4730

Meiler J, Prompers JJ, Peti W, Griesinger C, Brüschweiler R (2001) Model-free approach to the dynamic interpretation of residual dipolar couplings in globular proteins. J Am Chem Soc 123:6098–6107

Mittermaier A, Kay LE (2006) New tools provide new insights in NMR studies of protein dynamics. Science 312:224–228

Salmon L, Bouvignies G, Markwick P, Lakomek N, Showalter S, Li DW, Walter K, Griesinger C, Brüschweiler R, Blackledge M (2009) Protein conformational flexibility from structure-free analysis of NMR dipolar couplings: quantitative and absolute determination of backbone motion in ubiquitin. Angew Chem Int Ed Engl 48:4154–4157

Schmidt JM, Blumel M, Lohr F, Ruterjans H (1999) Self-consistent (3)J coupling analysis for the joint calibration of Karplus coefficients and evaluation of torsion angles. J Biomol NMR 14:1–12

Showalter S, Brüschweiler R (2007a) Validation of molecular dynamics simulations of biomolecules using NMR spin relaxation as benchmarks: application to the AMBER99SB force field. J Chem Theory Comput 3:961–975

Showalter SA, Brüschweiler R (2007b) Quantitative molecular ensemble interpretation of NMR dipolar couplings without restraints. J Am Chem Soc 129:4158–4159

Tjandra N, Bax A (1997) Direct measurement of distances and angles in biomolecules by NMR in a dilute liquid crystalline medium. Science 278:1111–1114

Tolman JR (2002) A novel approach to the retrieval of structural and dynamic information from residual dipolar couplings using several oriented media in biomolecular NMR spectroscopy. J Am Chem Soc 124:12020–12030

Tolman J, Flanagan J, Kennedy M, Prestegard J (1995) Nuclear magnetic dipole interactions in field-oriented proteins: information for structure determination in solution. Proc Natl Acad Sci USA 92:9279–9283

Tolman JR, Flanagan JM, Kennedy MA, Prestegard JH (1997) NMR evidence for slow collective motions in cyanometmyoglobin. Nat Struct Biol 4:292–297

Ulmer TS, Ramirez BE, Delaglio F, Bax A (2003) Evaluation of backbone proton positions and dynamics in a small protein by liquid crystal NMR spectroscopy. J Am Chem Soc 125:9179–9191

Vogeli B, Ying J, Grishaev A, Bax A (2007) Limits on variations in protein backbone dynamics from precise measurements of scalar couplings. J Am Chem Soc 129:9377–9385

Vogeli B, Yao L, Bax A (2008) Protein backbone motions viewed by intraresidue and sequential HN-Halpha residual dipolar couplings. J Biomol NMR 41:17–28

Yao L, Vogeli B, Torchia DA, Bax A (2008a) Simultaneous NMR study of protein structure and dynamics using conservative mutagenesis. J Phys Chem B 112:6045–6056

Yao L, Vogeli B, Ying J, Bax A (2008b) NMR determination of amide N-h equilibrium bond length from concerted dipolar coupling measurements. J Am Chem Soc 130:16518–16520